THE JOURNAL OF BIOLOGICAL CHEMISTRY VOL. 285, NO. 6, pp. 3928–3938, February 5, 2010

How *Escherichia coli* Is Equipped to Oxidize Hydrogen under Different Redox Conditions*[S]

Received for publication, September 18, 2009, and in revised form, October 30, 2009 Published, JBC Papers in Press, November 16, 2009, DOI 10.1074/jbc.M109.067751

Michael J. Lukey[‡1], Alison Parkin[‡1], Maxie M. Roessler[‡], Bonnie J. Murphy[‡], Jeffrey Harmer[‡], Tracy Palmer[§], Frank Sargent[§2], and Fraser A. Armstrong[‡3]

From the [‡]Department of Inorganic Chemistry, University of Oxford, South Parks Road, Oxford OX1 3QR, United Kingdom and the [§]College of Life Sciences, University of Dundee, Dow Street, Dundee DD1 5EH, Scotland, United Kingdom

The enterobacterium *Escherichia coli* synthesizes two H_2 uptake enzymes, Hyd-1 and Hyd-2. We show using precise electrochemical kinetic measurements that the properties of Hyd-1 and Hyd-2 contrast strikingly, and may be individually optimized to function under distinct environmental conditions. Hyd-2 is well suited for fast and efficient catalysis in more reducing environments, to the extent that *in vitro* it behaves as a bidirectional hydrogenase. In contrast, Hyd-1 is active for H_2 oxidation under more oxidizing conditions and cannot function in reverse. Importantly, Hyd-1 is O_2 tolerant and can oxidize H_2 in the presence of air, whereas Hyd-2 is ineffective for H_2 oxidation under aerobic conditions. The results have direct relevance for physiological roles of Hyd-1 and Hyd-2, which are expressed in different phases of growth. The properties that we report suggest distinct technological applications of these contrasting enzymes.

Hydrogenases catalyze the reversible cleavage of H_2 into protons and electrons, and play an important role in the energy metabolism of a broad range of microorganisms (1). Hydrogenases are classified according to their active site metal ion content, and three phylogenetically distinct classes have so far been identified: di-iron [FeFe]-, nickel-iron [NiFe]-, and mono-iron [Fe]-hydrogenases (1). Nickel-iron hydrogenases are the most abundant of the three types (1), and many members of this class are membrane bound, with the membrane-extrinsic domain consisting of a large subunit containing the active site, and a small subunit accommodating one to three electron-transferring iron-sulfur clusters. The active sites of [NiFe]-hydrogenases contain a nickel atom coordinated by four cysteine-S ligands, two of which bridge to an iron atom that is further coordinated by three unusual diatomic ligands, two cyanides and one carbonyl (2).

Hydrogenases are inactivated by O_2: reaction of the [NiFe] active site with O_2 results in at least two inactive Ni(III) forms, known as Ni-A ("unready") and Ni-B ("ready"). The ratio of these forms depends upon the conditions (especially the availability of electrons) under which O_2 attacks, and varies from one enzyme to another (3, 4). The unready state appears to contain a product of partial reduction of O_2 (a coordinated peroxide has been assigned (2, 5)) and it is re-activated only slowly upon reduction in the presence of H_2 (3). In contrast, the ready state contains a bridging hydroxo ligand (2, 6, 7) (the product of complete reduction of O_2) and is rapidly reactivated upon reduction (8).

Hydrogen plays a critical metabolic role in bacteria ranging from the strictly anaerobic, such as *Desulfovibrio* species (9), to the facultative aerobic, such as *Ralstonia* species (10). Furthermore, microaerophilic and facultative aerobic human pathogens, such as *Helicobacter* and *Salmonella*, respectively, are now known to require H_2 oxidation activity for virulence (11, 12). Thus, whereas the majority of well characterized [NiFe]-hydrogenases are inactivated by very low levels of molecular O_2 (4), in certain species there is a requirement for H_2 oxidation to occur in microaerobic and even fully aerobic environments. Hydrogenases capable of operating under aerobic conditions are defined as "O_2 tolerant" (13). To be O_2 tolerant a hydrogenase requires certain mechanistic features for dealing with O_2 attack, such as suppressing O_2 access to the active site (14), avoiding the formation of the unready state (Ni-A) and ensuring that any ready state (Ni-B) formed is reactivated rapidly (13).

The enterobacterium *Escherichia coli* synthesizes at least three [NiFe]-hydrogenases (15). Hydrogenase-3 (Hyd-3) is a cytoplasmic enzyme and forms part of the membrane-anchored formate hydrogen lyase system, which is responsible for H_2 evolution under fermentative conditions (16). In contrast, both Hyd-1 and Hyd-2 are membrane-bound periplasmic proteins, and are believed to function as "H_2-uptake" enzymes (17, 18). Hyd-1 is encoded by the first two genes of the *hyaABCDEF* operon, with *hyaA* coding for the [FeS] cluster-containing β-subunit and *hyaB* coding for the α-subunit, which binds the [NiFe] active site (19). Similarly, Hyd-2 is encoded by genes *hybO* and *hybC* of the *hybOABCDEFG* operon, with *hybO* coding for the β-subunit and *hybC* coding for the α-subunit (20). A membrane-anchoring hydrophobic helix is located at the extreme C terminus of the β-subunit of each enzyme. Hyd-1 couples H_2 oxidation to quinone reduction via the HyaC transmembrane cytochrome *b* (19), whereas Hyd-2 utilizes a

* This work was supported by United Kingdom Biotechnology and Biological Sciences Research Council Grants P15018 and BB/H001190/1 (to F. S.) and BB/D52222X and BB/H003878/1 (to F. A. A.), the Engineering and Physical Sciences Research Council (Supergen V (to F. A. A.) and EP/D0448559/1 supporting the Centre for Advanced Electron Spin Resonance), the Royal Society through a University Research Fellowship (to F. S.), and a Merton College, Oxford, Junior Research Fellowship (to A. P.).

[S] The on-line version of this article (available at http://www.jbc.org) contains supplemental Figs. S1–S4.

[1] Both authors contributed equally to this work.

[2] To whom correspondence may be addressed. E-mail: F.Sargent@dundee.ac.uk.

[3] To whom correspondence may be addressed. E-mail: fraser.armstrong@chem.ox.ac.uk.

periplasmic ferredoxin (HybA) to reduce quinone via the HybB integral membrane protein (21).

Regulation of the expression of Hyd-1 and Hyd-2 is distinct and complex. According to the available data, syntheses of both enzymes are repressed under aerobic conditions (22), but significant differences exist in the finer control of production. Repression by nitrate (23) or phosphate (24), stationary phase induction (25), and induction by acidic conditions (26) are all reported for the *hya* operon. In contrast, the *hyb* operon is expressed most strongly during the exponential phase of growth, and its expression is possibly catabolite repressed (23).

It has been proposed that the physiological role of Hyd-2 is to catalyze the oxidation of extraneous H_2, with the resulting electrons eventually being used by fumarate reductase to produce succinate (15). Thus Hyd-2 allows *E. coli* to use H_2 as an energy source during growth on non-fermentable carbon compounds. The physiological role of Hyd-1 is yet to be firmly established, but is believed to be quite distinct from that of Hyd-2. A suggested function of Hyd-1 is the *recycling* of H_2 produced by Hyd-3 under fermentative conditions (16). Additionally, evidence has emerged to suggest that Hyd-1 might be involved in linking H_2 oxidation to O_2 reduction under certain conditions (27). Indeed, a fragment of Hyd-1 has been purified from aerobically grown *E. coli*, implying that conditions might exist under which this enzyme is expressed in the presence of high concentrations of O_2 (28).

In protein film electrochemistry (PFE),[4] an extremely small quantity of redox protein is adsorbed directly onto an electrode to give a mono- or submonolayer film. A wealth of information can be obtained from enzymes, provided that full catalytic and electron-transfer activities are maintained in the adsorbed state (29). The *electro*catalytic activity of adsorbed enzymes responds directly to the electrode potential, and is monitored through the electrical current recorded in the presence of substrate. The current relates directly to the turnover frequency of the enzyme at the particular potential applied. Rates of change of catalytic state induced by stepping the electrode potential or introducing an inhibitor are measured from a current-time course. The environment of the adsorbed enzyme typically consists of 2 ml of enzyme-free buffer/electrolyte solution in a sealed electrochemical cell, through which precise mixtures of gases can be passed. Rotation of the electrode at controlled high speeds ensures that the observed reactions are not diffusion controlled, and also allows product inhibition to be quantified and suppressed (30).

In this article we describe the characterization of *E. coli* hydrogenases 1 and 2 and report striking differences in the catalytic properties of the two enzymes, most notably their contrasting activities under the different redox conditions and oxidizing environments likely to be encountered by the organism.

EXPERIMENTAL PROCEDURES

Bacterial Strains and Growth Conditions—The *E. coli* K-12 strains used in this study were FTH004 and FTH013, which are based on MC4100 (31). FTH004 (21) carries an engineered *hyaABCDEF* operon encoding a modified HyaA protein bearing a His_6 affinity tag at its extreme C terminus, whereas FTH013 carries an engineered *hybOABCDEFG* operon encoding a similarly modified HybO protein. FTH013 was constructed by PCR-amplifying a 500-bp fragment covering the 3′ end of the *hybO* gene (minus stop codon), digesting with XbaI and BglII, and cloning into pFAT210 (21). Next, a 500-bp fragment covering the 5′ region of the *hybA* gene (including the *hybA* ribosome binding site) was amplified by PCR, digested with ClaI and KpnI, and cloned into the pFAT210 construct. The $hybO^{his}$ allele now present on pFAT210 was then moved as an XbaI-KpnI fragment onto pMAK705 (32) before being transferred to the chromosome of MC4100 (32). The chromosomal modifications were carefully constructed so as to preserve identifiable regulatory elements, coding sequences, stop codons, and ribosome binding sites of genes flanking the *hyaA* and *hybO* loci.

FTH004 and FTH013, respectively, produce His-tagged Hyd-1 and His-tagged Hyd-2 at wild-type levels under native regulatory and biosynthetic control. The bacteria were cultured anaerobically at 37 °C in LB medium supplemented with 0.5% (w/v) glycerol and 0.4% (w/v) sodium fumarate. The inoculum (1%) was grown aerobically at 37 °C in LB medium. To isolate Hyd-1, cells were harvested during the stationary phase (centrifugation at 3,500 × *g* for 15 min at 4 °C). To isolate Hyd-2, the cells were harvested similarly, but during late exponential phase.

Isolation of the Membrane-bound Hydrogenases—The procedure for isolating His-tagged hydrogenase was essentially the same for both Hyd-1 and Hyd-2. All steps were carried out at 4 °C or on ice. The pelleted cells (FTH004 or FTH013) were resuspended in 100 mM Tris, pH 7.5, 1 mM EDTA, 50 mM NaCl, supplemented with 10 μg ml^{-1} of DNase I and 50 μg ml^{-1} of lysozyme (both from Sigma), and Complete EDTA-free protease inhibitor mixture tablets (Roche Molecular Biochemicals) at the manufacturer's recommended concentration.

The cells were disrupted by three passages through a French pressure cell, and crude membrane fractions were prepared by differential centrifugation as described (33). The pelleted membrane fraction was resuspended in 10 ml of 100 mM Tris, pH 7.5, 50 mM NaCl, and the suspension adjusted to a protein concentration of 10 mg ml^{-1} in the same buffer. Protease inhibitor mixture tablets were again added at the appropriate concentration.

The detergent *n*-dodecyl-β-D-maltoside was added to the suspension at a concentration of 1 mg/mg of protein, and the membranes were solubilized by gentle agitation at 4 °C overnight. Insoluble material was removed by ultracentrifugation at 150,000 × *g* for 1 h. Dithiothreitol was added to the cleared supernatant (giving 1 mM), and the solution was applied to a Ni^{2+}-loaded 5-ml HisTrap Chelating HP column (Amersham Biosciences) equilibrated in 20 mM Tris, pH 7.5, 150 mM NaCl, 50 mM imidazole, 1 mM dithiothreitol, 0.02% (w/v) *n*-dodecyl-β-D-maltoside (buffer A). The column was washed with 50 ml of buffer A and then developed in 40 ml of the same buffer using a linear gradient of imidazole to a final concentration of 500 mM. Fractions containing purified Hyd-1 or Hyd-2 as judged by SDS-PAGE followed by Coomassie Blue staining were pooled and subjected to two rounds of dialysis against 500 ml of buffer A containing no imidazole. The purified protein was then con-

[4] The abbreviation used is: PFE, protein film electrochemistry.

centrated by ultrafiltration, snap-frozen, and stored in liquid nitrogen.

Spectrophotometric Assays of Hydrogenase Activity—To measure H_2 uptake, the reduction of benzyl viologen (1 mM) (ϵ = 7.4 mM^{-1} cm^{-1}) was followed at 604 nm in anaerobic cuvettes containing 1 ml of 50 mM Tris/HCl, pH 7.0, 100 mM NaCl, saturated with H_2. Appropriate amounts of purified enzyme (5–50 μg) were injected to initiate the reaction. To measure H_2 production, the oxidation of methyl viologen (1 mM, pre-reduced with an equivalent of sodium dithionite) (ϵ = 13.7 mM^{-1} cm^{-1}) was followed at 604 nm in anaerobic cuvettes containing the same buffer, saturated with N_2.

Protein Film Electrochemistry Experiments—Pyrolytic graphite "edge" electrodes were constructed in-house (30). The pyrolytic graphite edge electrode surface is rich in hydrophilic C-O groups that bind many enzymes strongly with full retention of activity (34, 35). The electrode (geometric surface area 0.03 cm^2) was prepared by sanding with P800 Tufbak Durite sandpaper. Enzyme solution (2 μl at ~20 μM) was then pipetted onto the surface and, after 15 s, the electrode was held under a stream of water to remove non-adsorbed enzyme. All solutions used in the electrochemical cell are enzyme free, and therefore only enzymes adsorbed on the electrode and under the direct control of the electrode potential was examined. A mixed buffer system was used (8).

Electrochemical experiments were conducted in an all-glass cell located in an anaerobic glove box (Vacuum Atmospheres, O_2 <2 ppm). The saturated calomel reference electrode (SCE) was housed in a side-arm linked to the main compartment by a Luggin capillary. All potential values were corrected to the standard hydrogen electrode (SHE) scale using the relationship $E_{SHE} = E_{SCE} + 0.241$ V at 25 °C (36). The cell was sealed to a glass head fixed around an electrode rotator (EG&G). Gas inlet and outlet connectors allowed gas flow through the headspace. The electrode was rotated at variable high speed to control mass transport and ensure rapid equilibration of the cell solution with the head gas atmosphere. Precise gas mixtures were made using flow meters (Sierra Instruments). The total gas flow rate was typically 1000 standard cubic centimeters min^{-1}. The cell was water-jacketed and thermostated by a water circulator (Neslab). Kinetic analyses of hydrogenase inhibition by product and CO are described under supplemental data.

EPR Measurements and Data Analysis—Continuous wave EPR experiments were performed either using an X-band (9–10 GHz) Bruker EMX spectrometer (Bruker BioSpin GmbH, Germany) equipped with an X-band Super High Sensitivity Probehead (Bruker), or a W-/X-band Bruker Elexsys 680 spectrometer using an X-band EMX High Sensitivity Probehead (Bruker), both equipped with a low temperature helium flow cryostat (Oxford Instruments CF935). For determining *g* values, the magnetic field was calibrated at room temperature with an external 2,2-diphenyl-1-picrylhydrazyl standard (*g* value 2.0036). Data analysis and simulations of the EPR spectra were performed using the program *EasySpin* (37).

RESULTS

Isolation of Hydrogenase-1 and Hydrogenase-2 from E. coli—His_6-tagged Hyd-1 and Hyd-2 were expressed from the chromosome of *E. coli* strains FTH004 and FTH013, respectively, at wild-type levels. Hyd-1 was purified from the solubilized membrane fraction to near homogeneity in a single affinity chromatography step, with a yield of ~0.15 mg of protein (g of cells)$^{-1}$. Hyd-2 was purified in a complex with its physiological redox partner HybA, again with low levels of contamination, with a yield of ~0.015 mg of protein (g of cells)$^{-1}$. SDS-PAGE analyses of both enzymes are shown in supplemental Fig. S1. Spectrophotometric activity assays of purified Hyd-1 and Hyd-2 yielded specific activities for H_2 uptake of 1 μmol of H_2 min^{-1} mg^{-1} and 34 μmol of H_2 min^{-1} mg^{-1}, respectively. No H_2 production by Hyd-1 was detected, but a specific activity of 2.5 μmol of H_2 min^{-1} mg^{-1} was measured for Hyd-2.

Cyclic Voltammetry Experiments on Hyd-1 and Hyd-2—Both Hyd-1 and Hyd-2 are highly active in catalyzing H_2 oxidation. Fig. 1 shows electrochemical experiments on Hyd-1 and Hyd-2, each adsorbed as a film on a pyrolytic graphite edge electrode, at pH 6.0, 30 °C under three different H_2 partial pressures (10, 3, and 0.3% H_2 in argon). The cyclic voltammograms were initiated at −0.560 V and the electrode potential was steadily increased to +0.244 V at a rate of 1 mV s^{-1}. The scan direction was then reversed, and the potential lowered back to −0.560 V. Positive current is a direct measure of the net rate of steady-state H_2 oxidation ($H_2 \rightarrow 2H^+ + 2e^-$), and negative current, similarly, provides a direct, net measurement of the reverse reaction, H_2 production (30). The underlying wave shapes for electrocatalysis by enzymes have been explained previously (38, 39).

Important differences between the catalytic activities of the two enzymes are immediately apparent. The first of these differences relates to catalytic "bias" (the inherent ability to catalyze in one direction *versus* the other): whereas no H_2 production by Hyd-1 can be detected, Hyd-2 shows significant catalysis of this process.

The second difference relates to the ease of re-activation of the oxidized, inactive ready (Ni-B) state, which is formed under anaerobic oxidizing conditions (8, 40). The Ni-B state contains Ni(III) with a OH^- ligand in a bridging position (2). When the potential is scanned from a high (positive) value back to a low (negative) value, Ni-B reductively re-activates (a one-electron reduction of Ni(III) to Ni(II)); this reactivation is observed as an increase in current on the reverse scan, marked with asterisks in Fig. 1, *top panel*. The midpoint potential of reactivation is defined by the value E_{switch} determined from the derivative di/dE (8). At pH 6.0, E_{switch} is +0.150 V for Hyd-1 and −0.085 V for Hyd-2, showing that the inactive Ni-B state is much less favored thermodynamically in Hyd-1 than in Hyd-2. Therefore, at equilibrium at a potential of, for instance, 0 V, Hyd-1 would exist entirely in its active state, whereas Hyd-2 would be entirely in its inactive state.

The current trace for Hyd-2 crosses the zero line sharply and, under 10% H_2, this occurs at a potential of −0.33 V, the value predicted by the Nernst equation for the $2H^+/H_2$ redox couple (the reversible cell potential) under these conditions. However,

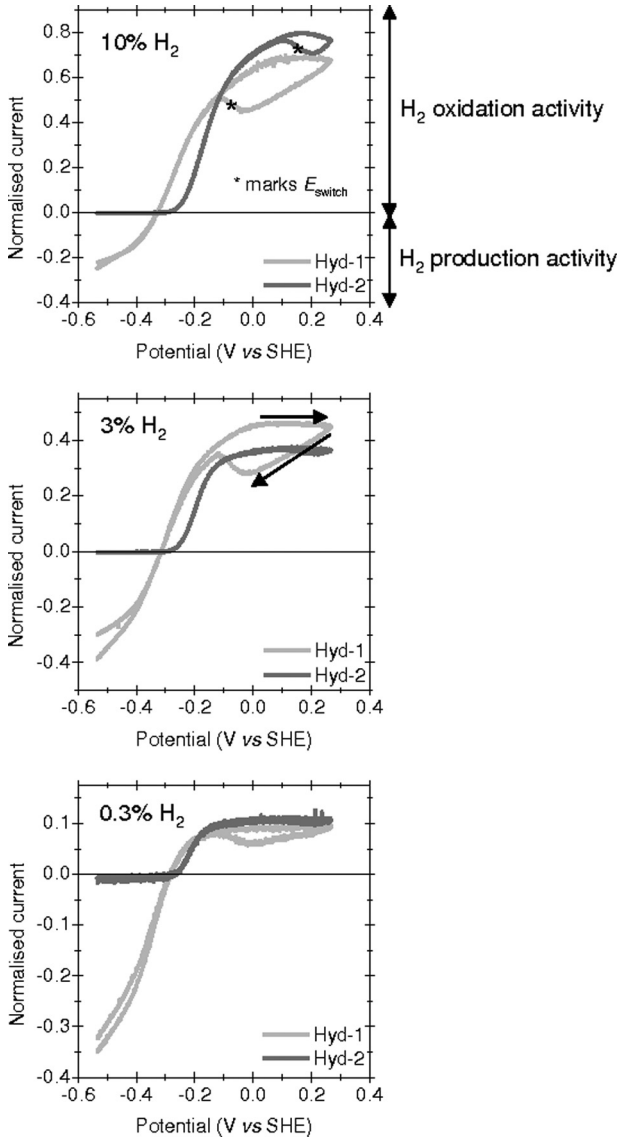

FIGURE 1. **The activity of *E. coli* hydrogenases-1 and -2 on a pyrolytic graphite edge electrode.** Cyclic voltammograms were recorded at 30 °C, pH 6, scan rate, 1 mV s^{-1}; total gas flow rate, 1000 standard cubic centimeters min^{-1}; electrode rotation rate, 8500 rpm, except under 0.3% H_2, when it was 9500 rpm. Hyd-1 results are indicated by *dark gray traces* and Hyd-2 results are indicated by *light gray traces*. *Top panel* shows voltammograms recorded under 10% H_2 in argon; *middle panel* shows voltammograms recorded under 3% H_2 in argon; and *bottom panel* shows voltammograms recorded under 0.3% H_2 in argon. *Asterisks* in the *top panel* indicate the potential E_{switch}, and *single-headed arrows* in the *middle panel* indicate the scan direction. As indicated in the *top panel*, the negative current is a direct measurement of enzyme-catalyzed H_2 production, and the positive current is a direct measure of enzyme-catalyzed H_2 oxidation. Maximum currents were normalized to those of the same sample under 100% H_2, which was measured prior to each voltammogram. Blank voltammograms, not shown, recorded using a bare pyrolytic graphite edge electrode with no enzyme adsorbed on the surface, showed that no H_2 oxidation or H^+ reduction occurs directly on the electrode surface. *SHE*, standard hydrogen electrode.

trace for Hyd-1 shows that H_2 oxidation under 10% H_2 becomes apparent only above a potential of −0.28 V, significantly more positive than the $2H^+/H_2$ cell potential. Hyd-1 therefore requires an *overpotential* of ~0.05 V to begin catalysis of H_2 oxidation under these conditions. Using the Hyd-2 voltammogram as a reference for the reversible cell potential, a close examination of Fig. 1 shows that the overpotential required for H_2 oxidation by Hyd-1 decreases as the partial pressure of H_2 is lowered.

A comparison of all three panels of Fig. 1 also reveals the sensitivity of Hyd-1 and Hyd-2 to changes in the partial pressure of H_2. Oxidation of H_2 by each enzyme is affected to a similar degree by changes in substrate concentration, and this implies that Hyd-1 and Hyd-2 have H_2 affinities of the same order of magnitude. Indeed, by carrying out Hanes analyses on data recorded at seven different H_2 concentrations, K_m values of 9 ± 1 and 17 ± 4 μM were determined for Hyd-1 and Hyd-2, respectively, at −0.175 V (see supplemental Fig. S2). From separate experiments to examine product inhibition of the H_2 production activity of Hyd-2, the inhibition constant $K_i^{H_2}$ was measured to be 210 ± 19 μM at pH 6.0, 30 °C, and −0.600 V (see supplemental Fig. S3). H_2 is therefore a weak product inhibitor of Hyd-2. Hyd-1 shows negligible H_2 production activity, even under a 100% argon atmosphere. Hyd-1 is thus exclusively a H_2 oxidizer, whereas Hyd-2 is, at least *in vitro*, a bidirectional hydrogenase.

Electron Paramagnetic Resonance Spectroscopy and PFE Analysis of As-isolated Hyd-1 and Hyd-2—Fig. 2 shows the X-band continuous wave EPR spectra of *as-isolated* samples of Hyd-1 and Hyd-2, each recorded at 10 K and 80 K. At 10 K, both Hyd-1 and Hyd-2 spectra are dominated by the strong signal of the $[3Fe\text{-}4S]^+$ cluster with g values (Hyd-1/Hyd-2: g_x = 2.02/2.03, g_y = 2.01/2.02, g_z = 2.00/2.01) consistent with those reported for [NiFe]-hydrogenases (*e.g.* Refs. 41–46). The spectrum of Hyd-1 is more complicated than that of Hyd-2, and we discuss this below.

At 80 K, only the EPR signals arising from nickel are observable, and can be examined without interference from the $[3Fe\text{-}4S]^+$ cluster, which relaxes rapidly at this temperature. The spectra show that both Hyd-1 and Hyd-2 form Ni-A *and* Ni-B states upon aerobic isolation. The rhombic signals characteristic of both Ni-A and Ni-B show identical g values (to two decimal places) for Hyd-1 and Hyd-2 (Ni-A, $g_x = 2.31$, $g_y = 2.24$, and $g_z = 2.01$; Ni-B, $g_x = 2.31$, $g_y = 2.16$, and $g_z = 2.01$). These values are in good agreement with those previously reported for [NiFe]-hydrogenases (6), although we consistently observed relatively more Ni-B than was evident in the data presented by DerVartanian *et al.* (47). The exact ratio of Ni-A to Ni-B varies between preparations: in the spectra shown, the ratio is ~1:3 for Hyd-1 and 1:4 for Hyd-2.

The spectra of Hyd-2 contain no signals apart from those arising from Ni-A, Ni-B, and $[3Fe\text{-}4S]^+$, and are similar to those of the [NiFe]-hydrogenases from *Desulfovibrio* sp. (46, 48–50). In contrast, the spectra of Hyd-1 contain several other peaks around the $[3Fe\text{-}4S]^+$ cluster region at g = 2.06, 1.96, 1.93, 1.91, and 1.87 (denoted with an *asterisk* in Fig. 2) as well as around the peaks arising from Ni-A and Ni-B at g = 2.36, 2.27, and 2.21 (indicated with an *open circle*). These features have been observed previously for [NiFe]-hydrogenases from *Allochromatium vinosum* (41, 51–53), *Thiocapsa roseopersicina* (42), and most recently *Ralstonia eutropha* (43). Interestingly, the peaks denoted with the *open circle* in Fig. 2 at the low-field end of the 10 K spectrum (which do not overlap with the $[3Fe\text{-}4S]^+$ cluster signals) are still present at 80 K, and thus there is no

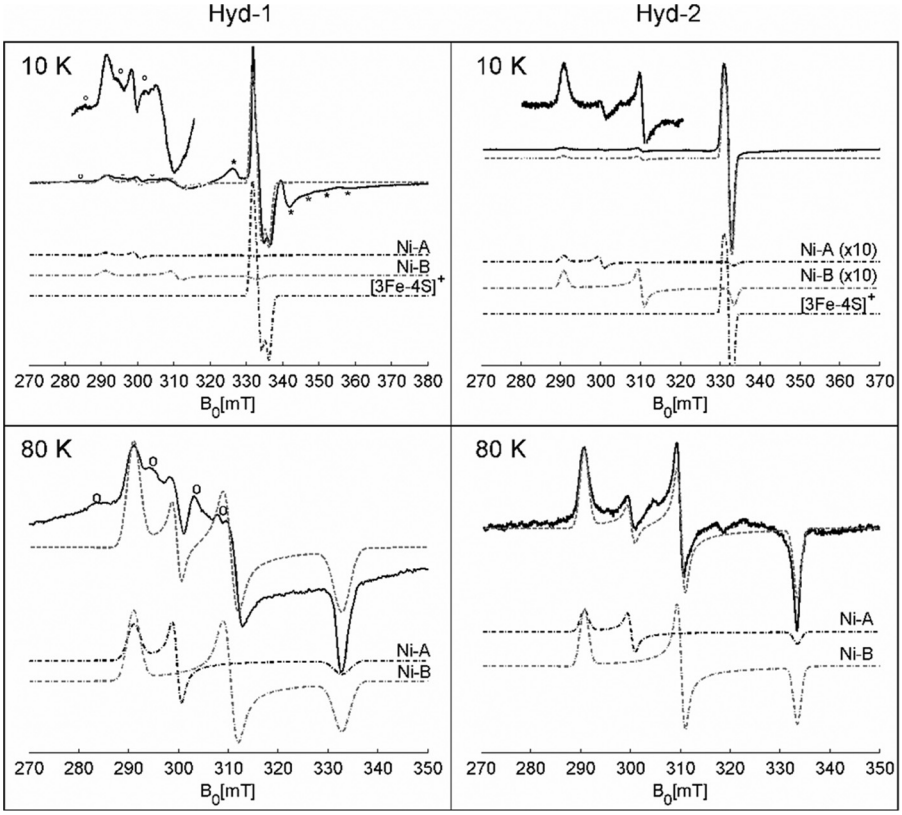

FIGURE 2. **X-band continuous wave EPR spectra of as-isolated *E. coli* Hyd-1 and Hyd-2.** *10 K*, microwave power 0.13 milliwatt; modulation amplitude 0.6 millitesla; *80 K*, microwave power 2.0 milliwatts; modulation amplitude 1.0 millitesla (Hyd-1)/0.5 millitesla(Hyd-2). * and ○ denote presently unexplained peaks (see text). *g* values (Hyd-1 and Hyd-2): Ni-A, $g_x = 2.31$, $g_y = 2.24$, and $g_z = 2.01$; Ni-B, $g_x = 2.31$, $g_y = 2.16$, and $g_z = 2.01$; $[3Fe\text{-}4S]^+$(Hyd-1/Hyd-2), $g_x = 2.03/2.03$, $g_y = 2.01/2.02$, and $g_z = 2.00/2.01$. The overall simulations, and the individual simulations of the components Ni-A, Ni-B, and $[3Fe\text{-}4S]^+$, are shown as *dotted lines*. When necessary, spectra were baseline subtracted using a baseline spectrum recorded under the same conditions as the spectrum of the enzyme sample.

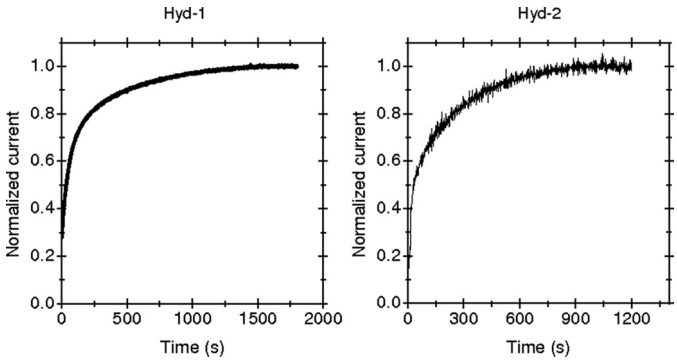

FIGURE 3. **Chronoamperometry traces showing the activation of as-isolated Hyd-1 and Hyd-2.** Chronoamperometry traces show activation of as-isolated samples of Hyd-1 and Hyd-2 during their first exposure to an atmosphere of 100% H_2 following aerobic purification. Measurements were made at pH 6.0, 30 °C, 100% H_2, at a potential of −0.060 V in the case of Hyd-1, and −0.200 V in the case of Hyd-2 (both potentials below E_{switch} of the respective enzyme).

evidence of a spin-spin interaction between the [NiFe] center and the $[3Fe\text{-}4S]^+$ cluster.

Fig. 3 shows plots of current against time (chronoamperometry), which reveal reductive activation of *as-isolated* samples of Hyd-1 and Hyd-2 during their first exposure to H_2 after aerobic purification. The measurements were made at pH 6.0, 30 °C, by holding the electrode potential at a value more negative than E_{switch} (−0.060 V was chosen for Hyd-1, and −0.200 V for Hyd-2), to drive the reductive reactivation process. In electrochemical experiments Ni-A is identified by slow activation kinetics (hence the term unready), whereas Ni-B always activates much more rapidly (3). Such experiments are therefore complementary to the EPR described above for comparing the relative amounts of Ni-A and Ni-B. Activation of both Hyd-1 and Hyd-2 is biphasic: the first phase is fast and includes the activation of Ni-B, whereas the second phase is much slower and represents activation of Ni-A. Therefore, both EPR data and PFE experiments show that *as-isolated* Hyd-1 and Hyd-2 both contain Ni-A and Ni-B, and again, the ratio of these two species varies between preparations. Such chronoamperometry experiments provide only a qualitative comparison of the *as-isolated* enzymes, because the current-time relationship is complicated by the rate at which the enzyme becomes favorably oriented on the electrode following its application, because of relatively rapid film loss immediately after adsorption, and also because of the need to commence measurements as soon as the electrochemical cell was sealed, and before gas concentrations had equilibrated.

A Comparison of the Effects of O_2 at High Potential on Active Hyd-1 and Hyd-2—The cyclic voltammograms in Fig. 4*A* show that fully activated Hyd-1 responds to high-potential O_2 exposure in a dramatically different manner to Hyd-2. The left-hand voltammogram shows the response of Hyd-1 to O_2 under an atmosphere of 100% H_2. During the forward scan, O_2-saturated buffer was injected into the cell solution when the electrode potential reached 0.03 V, to give a total O_2 concentration of 144 μM. A sudden decrease in the current is observed, but the H_2 oxidation activity does not fall to zero. The decrease is attributable partly to enzyme inhibition, and partly to temporary dilution of H_2 in the cell solution. Importantly, there is a rapid recovery of activity, even though the sweep is continuing in the direction of more positive potential (see Fig. 4, *asterisk*), before the activity again begins to decrease. The continuing flow of H_2 through the cell headspace ensures that by the time the electrode potential has reached +0.244 V, almost all of the injected O_2 has been flushed from the cell solution. On the reverse sweep (to negative potential) the activity increases and reaches a maximum at ~0 V. The E_{switch} value of +0.150 V for recovery of Hyd-1 from aerobic inactivation is the same as that recorded

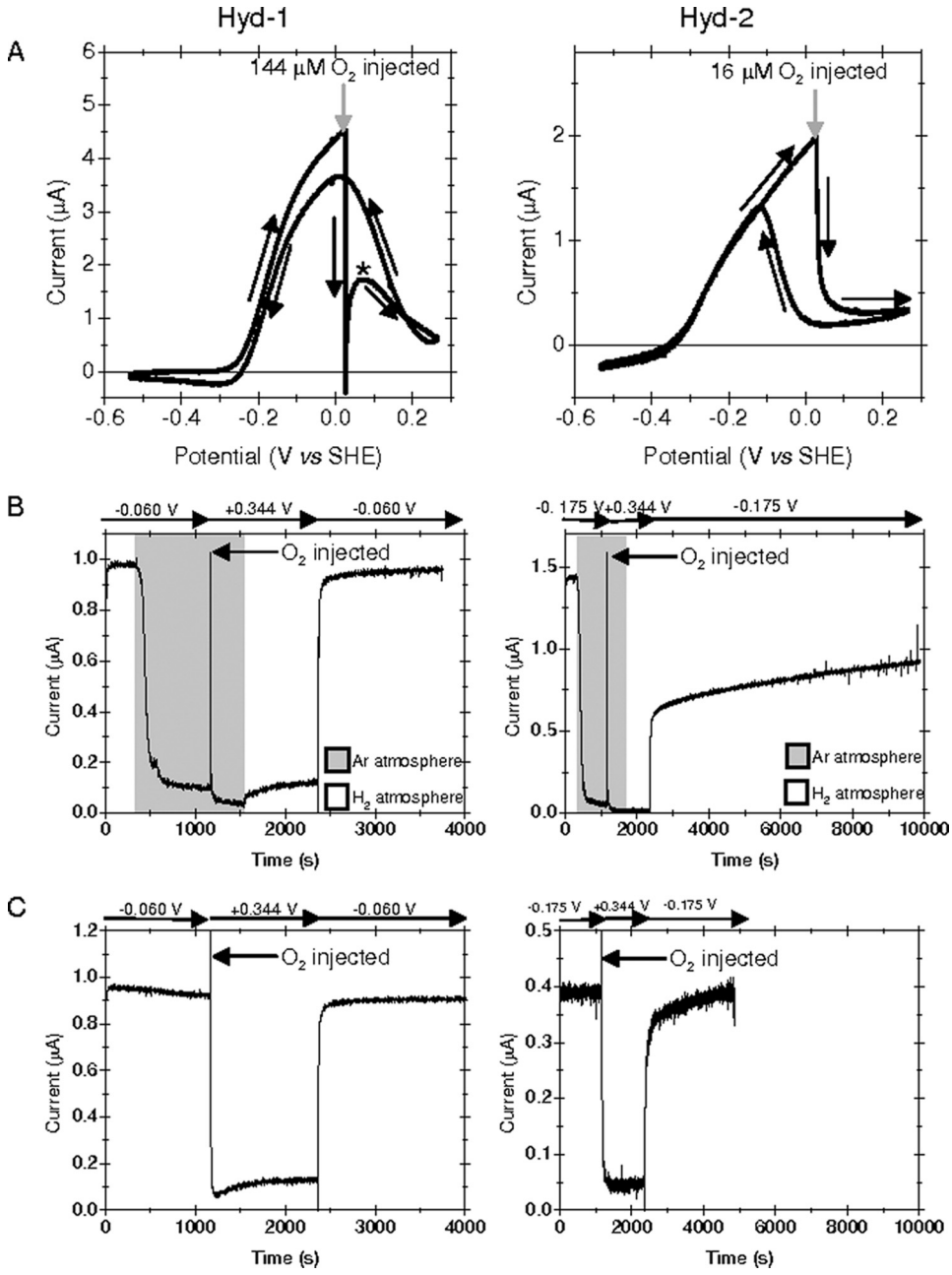

FIGURE 4. **A comparison of the O_2 tolerance of hydrogenases-1 and -2.** Cyclic voltammograms in *A* recorded at 30 °C, pH 6.0, scan rate 1 mV s^{-1}, under 100% H_2. *Black arrows* mark scan direction, and labeled *gray arrows* mark the point of O_2 injection. Chronoamperometry traces in *B* and *C* were recorded at pH 6.0, 30 °C, under either 100% H_2 (*white* background) or 100% argon (*gray* background). Potentials are as indicated. The cyclic voltammograms in *A* show the response of Hyd-1 and Hyd-2 to O_2 at high potential. In the case of Hyd-1, at 0.03 V on the forward sweep, O_2-saturated buffer is injected into the cell solution to give an O_2 concentration of 144 μM. The O_2 concentration immediately begins to fall due to continued flushing of H_2; by the time the potential reaches +0.25 V and the scan direction reverses, most O_2 has been flushed from the cell. A similar experiment on Hyd-2 is shown, with all conditions the same except that 16 μM O_2 is injected at 0.03 V, instead of 144 μM. *B*, *left-hand side*: a chronoamperometry experiment to investigate the inhibited active site states of Hyd-1 after exposure to O_2 at high potential *in the absence of* H_2. An initial measure of the H_2 oxidation activity of the film is made under 100% H_2 (*white background*), and the system is then equilibrated with 100% argon (*gray background*). For the first 1200 s, the potential is held at −0.060 V. Immediately on stepping the potential to +0.344 V, O_2-saturated buffer is injected into the cell solution to give an O_2 concentration of 325 μM. After re-equilibrating the electrochemical cell with H_2 (*white background*), the potential is stepped back to −0.060 V. *B*, *right-hand side*: a similar experiment on Hyd-2, in which all conditions are the same, except that the initial and final potential is −0.175 V instead of −0.06 V. *C*, similar chronoamperometry experiments to those in *B*, but this time O_2 is injected under 100% H_2.

during recovery from anaerobic inactivation (Fig. 1); in both cases, the scan rate is very low, thus approaching as closely as possible reversible conditions.

The cyclic voltammogram on the right-hand side of Fig. 4*A* shows an experiment carried out on Hyd-2, in which all conditions were identical to those for Hyd-1 except for the amount of O_2 added to the electrochemical cell; this time, O_2-saturated buffer was injected to give an O_2 concentration of 16 μM, only one-ninth of the O_2 concentration to which Hyd-1 was exposed. The response of Hyd-2 shows that this enzyme is much more sensitive than Hyd-1 to O_2. Immediately upon addition of 16 μM O_2 at 0.03 V, the H_2 oxidation activity of Hyd-2 falls to less than 15% of the pre-O_2 activity. As the potential is scanned to more positive values and O_2 is flushed from the electrochemical cell, no recovery of Hyd-2 activity occurs. Furthermore, upon reversal of the scan direction, Hyd-2 does not reactivate until a much lower potential has been reached (−0.085 V) than that required for recovery of Hyd-1. Again, this E_{switch} value is the same as that measured for recovery of Hyd-2 from the anaerobically inactivated state (Fig. 1). Similar experiments, the results of which are shown in supplemental Fig. S4, reveal that exposure of each enzyme sample to 42 μM O_2 at high potential results in about 40% inhibition of Hyd-1 and 100% inhibition of Hyd-2.

Fig. 4 also shows potential step kinetic experiments that distinguish between differences in the composition of the O_2-inhibited states of Hyd-1 and Hyd-2, generated when active enzyme is exposed to O_2 at high potential, either under argon or H_2. Unlike the experiments in Fig. 3, the enzyme films have had time to become established on the electrode. In Fig. 4*B*, samples of Hyd-1 or Hyd-2 were first held under a headgas atmosphere of 100% H_2 at a potential significantly below E_{switch} but at which considerable H_2 oxidation activity can be observed (−0.060 V was chosen for Hyd-1 and −0.175 V for Hyd-2). This provided an initial measure of the catalytic current recorded from the particular enzyme film being studied. The headgas in the electrochemical cell was then changed from H_2

to argon, and the system was left for 800 s to equilibrate, still under control of the electrode potential; the current decreased as the substrate was purged from the solution, and reached a steady value by 1000 s. Because the $K_m^{H_2}$ of the enzymes is so low and glove box pressure was raised to permit injection of inhibitor, unavoidable leakage of trace amounts of H_2 into the electrochemical cell results in this steady-state current being higher than 0 A. The potential was next stepped to +0.344 V, and O_2-saturated buffer was immediately injected to give a final O_2 concentration of 325 μM in the cell solution. It was important to ensure that O_2 injection occurred exactly simultaneously with the step to high potential, as the aim of the experiment was to analyze the effect of O_2 on *active* enzyme; this makes it essential that no anaerobic inactivation occurs prior to O_2 exposure. The system was next held at +0.344 V for 1200 s, during which time the electrochemical cell re-equilibrated with H_2 and all O_2 was flushed from the cell solution. Finally, the potential was stepped back below E_{switch} (to −0.060 V for Hyd-1, and −0.175 V for Hyd-2), and the kinetics of reactivation of each enzyme were monitored.

Reactivation of both enzymes occurs in two phases, the first being very fast and corresponding to reactivation of Ni-B. In the case of Hyd-1, this accounts for ~85% of the increase in current. The second phase (~15%) represents the much slower reactivation of Ni-A, with a rate of 2×10^{-3} s^{-1} ($t_{½}$ 340 s at 30 °C). In the case of Hyd-2, only 55% of the observed reactivation is characteristic of Ni-B recovery, and the remaining reactivation occurs over a period of several hours and is characteristic of Ni-A recovery. Thus, under these identical O_2 exposure conditions (in the absence of H_2), Hyd-2 is more than twice as prone as Hyd-1 to forming the Ni-A state.

Similar experiments in which O_2 was injected under an atmosphere of H_2 instead of argon are shown in Fig. 4*C*. The presence of H_2, and the consequential greater electron availability, is known to enhance formation of Ni-B over Ni-A (3). The amount of Ni-A formed by Hyd-1 under these conditions is negligible, and although Hyd-2 still shows some Ni-A reactivation when the potential is lowered, the ratio Ni-A:Ni-B is less than one-third of that following O_2 exposure under a H_2-free atmosphere.

The Activity of Hyd-1 under Aerobic Conditions—The ability of Hyd-1 to reactivate from rapid O_2 inhibition at high potential, in conjunction with its low $K_m^{H_2}$ value, suggests that there should be a window of potential within which the enzyme can maintain H_2 oxidation under a low H_2 partial pressure and 20% O_2. Fig. 5 shows an experiment that proves that Hyd-1 is an O_2-tolerant H_2 oxidizer. The cyclic voltammograms were recorded at 1 mV s^{-1}, pH 6.0, 37 °C, under three different gas mixtures: 10% H_2, 90% argon; 10% H_2, 20% O_2, 70% argon; and 20% O_2, 80% argon. Before measurements were made, the cell was allowed to equilibrate for 15 min with the appropriate gas mixture at −0.560 V. Under 10% H_2 at −0.1 V, ~40% of the H_2 oxidation current measured in O_2-free conditions was sustained in the presence of 20% O_2. This value is actually a slight underestimate, because at potentials more negative than 0 V there is a negative contribution to the current due to direct reduction of O_2 at the graphite electrode surface, as shown in the scan recorded under 20% O_2, 80% argon.

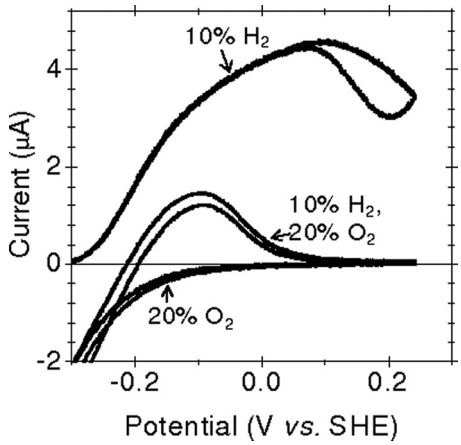

FIGURE 5. **Aerobic H_2 oxidation by Hyd-1.** Cyclic voltammograms recorded at 1 mV s^{-1}, pH 6.0, 37 °C, under three different gas mixtures: 10% H_2, 90% argon; 10% H_2, 20% O_2, 70% argon; and 20% O_2, 80% argon, a total flow rate 500 standard cubic centimeters min^{-1} in each case. Prior to each measurement, the cell was allowed to equilibrate for 15 min with the appropriate gas mixture. Note that an O_2 reduction current arises from direct reaction of O_2 with the electrode.

The Effect of CO on the Activity of Hyd-1 and Hyd-2—The classic inhibitor of H_2-cycling catalysts is CO (54). Fig. 6 shows experiments in which the inhibition constant $K_i(CO/H_2)$ was measured for Hyd-1 (*panel A*) and Hyd-2 (*panel B*) during H_2 oxidation at a fixed potential below E_{switch}, pH 6.0, 20 °C. Under a constant headgas atmosphere of 20% H_2 in argon, the concentration of CO was increased stepwise from 0 to 50%. To demonstrate reversibility of inhibition, CO was then flushed from solution; in the case of both Hyd-1 and Hyd-2, H_2 oxidation activity returned to the level recorded prior to CO exposure. A plot of i_{max}/i_t *versus* [CO], where i_{max} is the current recorded under 100% H_2 (measured prior to the experiment), gives a straight line of intercept $(K_m/[S]) + 1$ and gradient $K_m/(K_i \cdot [S])$ (see supplemental data). Such analyses are shown in the *insets* in Fig. 6. Under 20% H_2, $K_i(CO/H_2)$ values were measured to be 51 ± 6 μM for Hyd-1 at −0.060 V and 3 ± 1 μM for Hyd-2 at −0.175 V (both potentials are below E_{switch} of the respective enzymes). Thus Hyd-2, in addition to showing far greater sensitivity than Hyd-1 to O_2, is almost 20-fold more sensitive than Hyd-1 to inhibition by CO during H_2 oxidation. Fig. 6*C* shows a similar experiment to measure $K_i^{app}(CO/H^+)$ for Hyd-2 during H_2 production at −0.560 V, pH 6.0, 20 °C. The experiment was carried out under an argon atmosphere with increasing partial pressures of CO, and again inhibition was shown to be reversible. The analysis shown in the *inset* gives a gradient of $(1/K_i^{app}(CO))$, which allows the $K_i^{app}(CO/H^+)$ value to be calculated as 11 ± 3 μM at −560 mV.

The Effect of O_2 on the H_2 Production Activity of Hyd-2—For reasons explained in detail by Goldet *et al.* (55, 56), experiments to investigate the effect of O_2 on enzymes under very reducing conditions are subject to particular difficulties, most notably the reaction of soluble electron donors with O_2. These problems can be overcome using PFE, provided that hydrogenase-catalyzed H^+ reduction is distinguishable from O_2 reduction, which occurs directly on the electrode surface. By introducing a gaseous inhibitor such as CO, which is specific for the hydrogenase and has no effect on O_2 reduction at the electrode, the

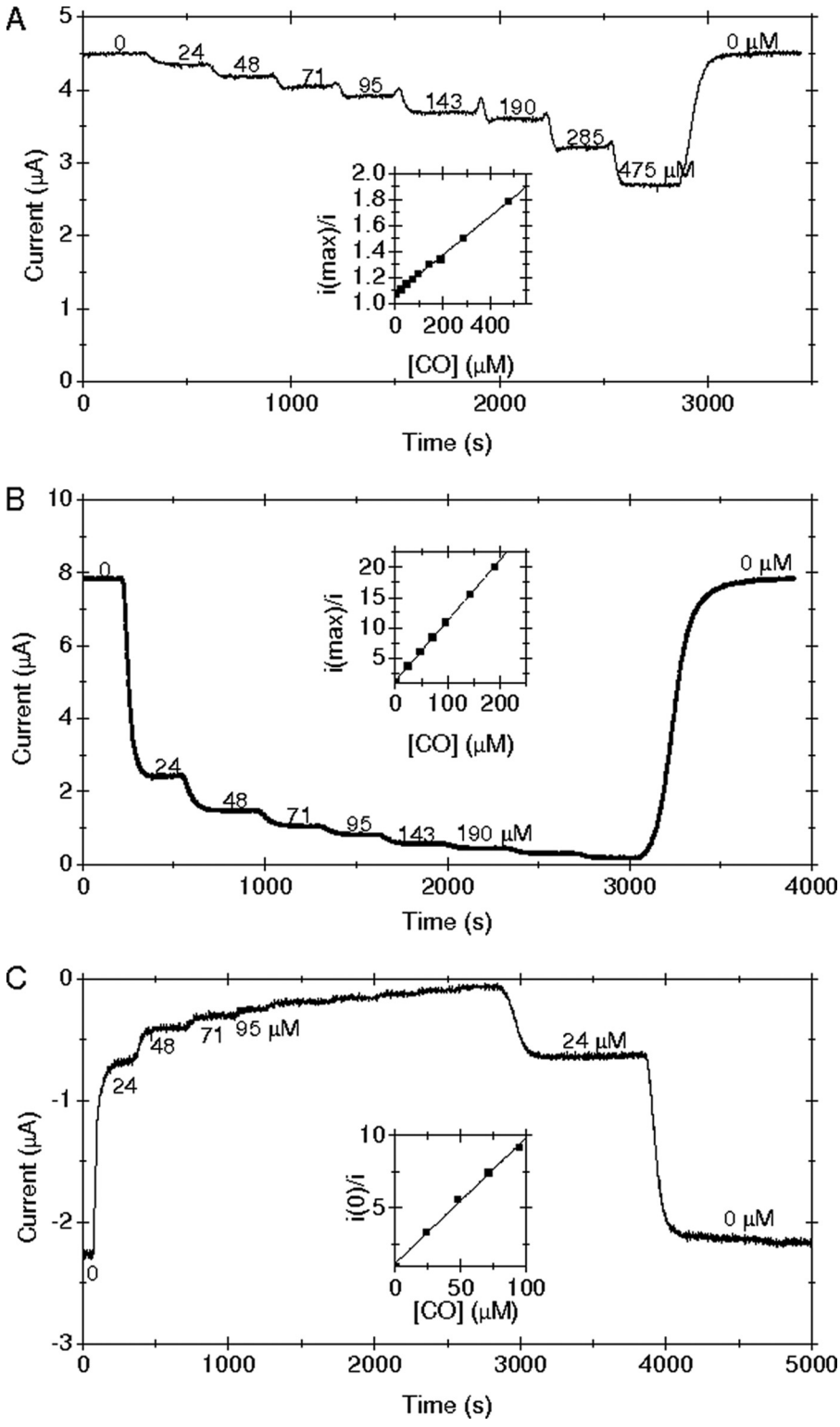

FIGURE 6. **Sensitivity of Hyd-1 and Hyd-2 to CO.** Chronoamperometry traces of Hyd-1 (*A*) and Hyd-2 (*B* and *C*) during exposure to varying CO concentrations, as indicated. Experimental conditions were: pH 6.0, 20 °C, electrode rotation rate 3500 rpm, and total gas flow rate 1000 standard cubic centimeters min^{-1}. *Panel A* (Hyd-1), electrode potential −0.060 V, carrier gas 20% H_2 in argon with increasing partial pressures of CO (the resulting concentration of CO in the electrochemical cell solution is indicated). *Panel B* (Hyd-2), electrode potential −0.175 V, carrier gas 20% H_2 in argon with increasing partial pressures of CO. *Panel C* (Hyd-2), electrode potential −0.560 V, carrier gas argon with increasing partial pressures of CO. In each case, CO is flushed from solution at the end of the experiment, to demonstrate reversibility of inhibition. *Insets* show plots used to determine K_i(CO) in each case (see "Results"). $K_i(CO/H_2)$ for H_2 oxidation by Hyd-1 (*A*) was measured to be 51 ± 6 μM; $K_i(CO/H_2)$ for H_2 oxidation by Hyd-2 (*B*) was 3 ± 1 μM; and $K_i^{app}(CO/H^+)$ for H_2 production by Hyd-2 (*C*) was 11 ± 3 μM.

H_2 production current resulting from enzyme catalysis can be extracted from the overall current.

Fig. 7 shows such an experiment. The measurement was initiated under a 100% argon atmosphere, and the negative current recorded corresponds only to H_2 production catalyzed by Hyd-2 on the electrode. Changing the headgas mixture to 10% CO in argon resulted in a rapid loss of current, due to inhibition of the enzyme. After recording the effect of this CO concentration, the headgas was changed back to 100% argon, and the H_2 production current recovered as CO was purged from solution.

In the next part of the experiment, the headgas was changed to 1.25% O_2 in argon (from Henry's law, this gives an O_2 concentration of 16 μM in the cell solution at 30 °C). A correction is required to allow for removal of O_2 by its direct reduction on the electrode surface. Using the method of Goldet *et al.* (55, 56), it was estimated that the O_2 concentration experienced by Hyd-2 under these conditions is $10 < [O_2] < 16$ μM. Non-enzymatic O_2 reduction produces an increase in negative current. Once a steady value was established, 10% CO was again added to the headgas. A rapid decrease in negative current occurred, due solely to specific CO inhibition of H_2 production by active enzyme; importantly, the magnitude of the current loss was very similar to that resulting from CO addition in the absence of O_2 in the previous stage. From this, it is concluded that the H_2 production activity of Hyd-2 is largely unaffected by the presence of the low level of O_2 ($10 < [O_2] < 16$ μM).

Upon switching the headgas back to 1.25% O_2 in argon, the negative current increased in magnitude as the inhibitory CO was flushed from solution. In the final stage, anaerobic conditions (*i.e.* 100% argon) were restored, and a further CO gas exchange was carried out to compare the activity of the enzyme after O_2 exposure to that recorded before. After 1750 s of catalysis in

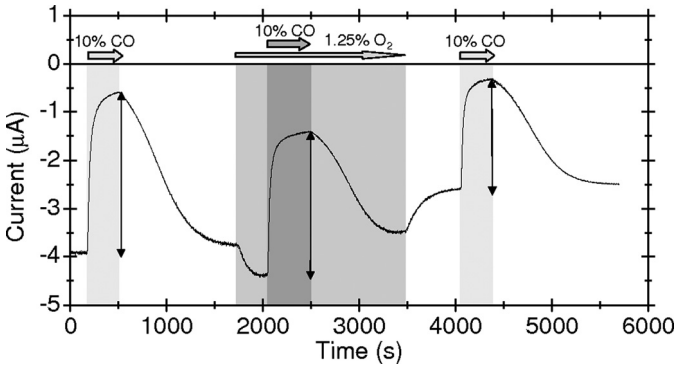

FIGURE 7. **O_2-tolerant H_2 production catalyzed by Hyd-2.** Experimental conditions were: pH 6.0, 25 °C, electrode potential −0.560 V, electrode rotation rate of 3500 rpm. Argon is the carrier gas, and CO and O_2 are introduced into the headspace at the times and concentrations indicated. *Double-headed arrows* indicate the magnitude of CO-inhibited H_2 production catalyzed by Hyd-2.

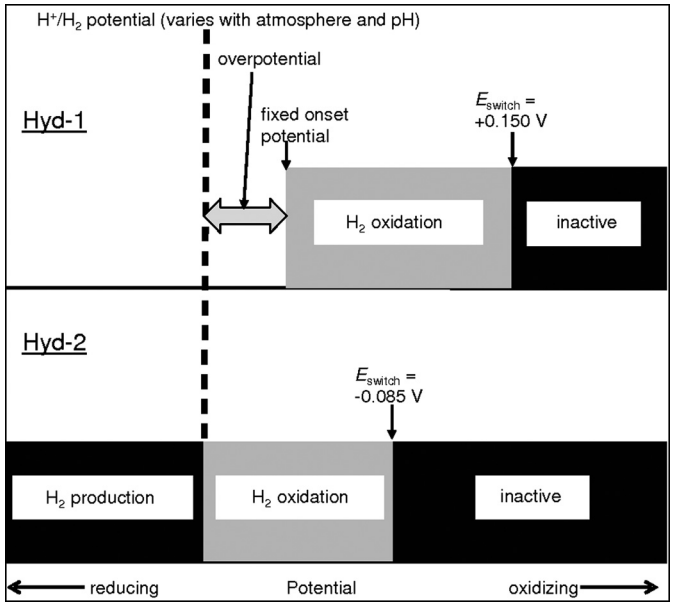

FIGURE 8. **Comparisons of the *in vitro* capabilities (represented as potential activity windows) of Hyd-1 and Hyd-2.** This is valid both under anaerobic conditions and upon exposure to O_2, provided that the product of inhibition is the Ni-B state and not Ni-A. E_{switch} values, as measured under 10% H_2, pH 6.0, 30 °C, are indicated.

the presence of O_2, ~70% of the initial H_2 production activity remained.

DISCUSSION

The strikingly different catalytic profiles of Hyd-1 and Hyd-2 are summarized in Fig. 8. The "activity window" for H_2 oxidation by hydrogenases is defined by the potential at which H_2 oxidation activity commences and the potential at which the enzyme anaerobically inactivates (4). Under anaerobic conditions, Hyd-2 shows high activity in more reducing environments, to the extent that it can *produce* as well as oxidize H_2 in electrochemical experiments. However, the active form of Hyd-2 is unstable at potentials more positive than −0.085 V because the inhibited Ni-B state is formed. In contrast, the H_2 oxidation activity window of Hyd-1 is shifted to more oxidizing potentials, and Hyd-1 shows no activity at potentials low enough for H_2 production. PFE is well suited for measuring relative catalytic bias (oxidation *versus* reduction) and the precise dependence of rates on potential, but it is often not possible to measure electroactive coverage (it is too low) and therefore absolute activities are difficult to determine. Conversely, solution assays can underestimate activity because of limitations due to the driving force and bimolecular encounters. The results obtained with benzyl viologen suggest that Hyd-1 is much less active than Hyd-2. This differential is at least partly explained by the voltammograms (Fig. 1) that show that Hyd-1 but not Hyd-2 requires an overpotential of ~50 mV before oxidation of H_2 commences: benzyl viologen ($E'_0 = -350$ mV) is only a very weak oxidant for H_2 at pH 6.0. The absence of detectable H_2 production by Hyd-1 using methyl viologen ($E'_0 = -460$ mV) also corresponds perfectly with our PFE results.

When O_2 reacts with the active site of [NiFe] hydrogenases, a more reducing environment favors the formation of Ni-B over Ni-A (3). A proficient supply of electrons is required to ensure that O_2 is rapidly and fully reduced to H_2O or equivalent species (OH^-), and that intermediates such as peroxide do not become trapped. When conditions prevail in which Ni-B is the dominant or sole species produced on reaction with O_2, the activity window of the enzyme in the presence of O_2 will be the same as that under anaerobic conditions. The upper limit is thus defined by the potential at which Ni-B is re-activated (E_{switch}). Furthermore, because the rate of reductive activation of Ni-B is much higher than that of Ni-A, a hydrogenase that forms negligible amounts of Ni-A upon exposure to O_2 will be O_2 tolerant (13). Under extended exposure to O_2 with no control of potential, as occurs during isolation, both Hyd-1 and Hyd-2 form Ni-A and Ni-B active site states in poorly reproducible ratios. However, during H_2 oxidation at a controlled electrode potential, the ratio Ni-B:Ni-A formed on exposure to O_2 is far greater in Hyd-1 than in Hyd-2. This, along with our measurement of a much more positive E_{switch} for Hyd-1 than for Hyd-2, correlates with our finding that Hyd-1 is a truly O_2-tolerant enzyme.

Hyd-1 and Hyd-2 are both located in the periplasm of *E. coli*, and thus are exposed to conditions that depend largely on the external environment. In particular, periplasmic O_2 levels will fluctuate considerably during the infection cycle of *E. coli*. The high potential of the activity window for Hyd-1 would correlate with the enzyme being expressed and utilized under more oxidizing conditions, and indeed Hyd-1 but not Hyd-2 has been detected in aerobically grown cultures of *E. coli* (28).

The contrast between the H_2 oxidation activities of Hyd-1 and Hyd-2 that is only evident from voltammetric experiments, namely that there is a region of potential in which Hyd-2 is operational and Hyd-1 is not, depends on H_2 concentration. This region is larger at higher H_2 levels, and diminishes so that at 0.3% H_2 the difference is smaller than 20 mV. The effect arises as a result of the overpotential requirement of Hyd-1 at higher H_2 levels, the origin of which is under investigation. Measurements at −0.175 V showed Hyd-1 to have a slightly lower K_m than Hyd-2. Physiological evidence implies that Hyd-1 may permit the coupling of H_2 oxidation to O_2 reduction by *E. coli* (27), and it is highly likely that whenever *E. coli* is exposed to O_2, H_2 levels will be very low. Therefore if Hyd-1 does oxidize H_2 in the presence of O_2 *in vivo*, the low K_m that we

measure would be a pre-requisite for significant energy extraction.

Hyd-2 behaves like a "standard" [NiFe]-hydrogenase on exposure to O_2 at high potential; like the hydrogenases from the *Desulfovibrio* species it cannot catalyze oxidation of H_2 in the presence of O_2, although the result shown in Fig. 6 reveals Hyd-2 to be capable of O_2-tolerant H_2 production. This is possible because H_2 production catalyzed by Hyd-2 occurs at potentials well below E_{switch} (in the experiment a potential of −0.560 V was used). Under such conditions, the [NiFe] active site of the enzyme has ready access to a continuous supply of electrons, facilitating recovery from the Ni-B product of attack by O_2. Also, at such negative potentials, only a small amount of Ni-A is ever likely to accumulate. Consequently, after almost 2000 s of exposure of active Hyd-2 to O_2 under H_2 production conditions, the majority of the enzymes pre-O_2 exposure activity remains.

In addition to their different catalytic biases and the distinct rates and potentials associated with their reactions with O_2, Hyd-1 and Hyd-2 are further distinguished by their EPR spectra. The presence of a split signal at $g = 2.01$ for Hyd-1 is similar to that observed for the [NiFe]-membrane-bound hydrogenase from *R. eutropha*, the best established O_2-tolerant hydrogenase to date (43). In contrast, the relatively simple spectrum of Hyd-2 resembles hydrogenases from *Desulfovibrio* (46, 48–50), which are strict anaerobes.

The data presented here not only demonstrate *how E. coli* can oxidize H_2 under different redox environments, but also suggests *why* this bacterium needs to express two separate uptake hydrogenases. Our physical characterization, taken together with genetic analyses (*e.g.* Refs. 19 and 57), establish that Hyd-1 is an O_2-tolerant, unidirectional H_2 oxidizer, the role of which seems to be H_2 scavenging under conditions of slow growth and fluctuating O_2 levels. The H_2 oxidation activity of Hyd-1 is probably tightly coupled to the generation of a proton motive force via a loosely associated transmembrane cytochrome *b* subunit (HyaC) (19). In this respect, Hyd-1 shares a predicted similar overall structure to the *R. eutropha* membrane-bound hydrogenase (58). The function of Hyd-1 as an energy-conserving enzyme perhaps explains why this isoenzyme demonstrates an inherent inability to catalyze H_2 production at low redox potentials: reverse electron transport from the quinol pool through the Hyd-1 complex *in vivo* would collapse the transmembrane electrochemical gradient. The unidirectional nature of Hyd-1 is therefore an important physiological feature.

The characterization here of Hyd-2 as a hydrogenase capable of bidirectional behavior also correlates with what is known about the genetics of this system. Hyd-2 is not thought to associate with a HyaC-type quinone reductase, but instead passes electrons to the quinone pool by a different route, without generating a proton electrochemical gradient (21, 59). It is possible that Hyd-2 is fine-tuned for conditions of rapid growth under nutrient-rich, but strictly anaerobic, conditions. Indeed, because Hyd-2 is uncoupled, this enzyme can potentially act as an electron release valve and run "backwards" if the quinone/quinol pool becomes over-reduced. Thus, Hyd-2 is not a suitable system for conserving energy by H_2 scavenging at high redox potentials, and vice versa, Hyd-1 is not suited to bi-directional activity at low redox potentials.

Finally we summarize some possible technological implications. If H_2 is to be harnessed as a fuel, H_2O-splitting catalysts must be designed. An enzyme such as Hyd-2, which can tolerate exposure to O_2 during H_2 production, proves the possibility of Pt-free catalysts for H_2 production under ambient conditions. The contrasting properties of Hyd-1 and Hyd-2 that we demonstrate are already being exploited in two completely different applications. The ability of Hyd-2 to produce H_2 in the presence of CO (although CO does act as an inhibitor, considerable enzyme activity remains under low CO partial pressures) has allowed Hyd-2 to be coupled to a CO dehydrogenase from *Carboxydothermus hydrogenoformans* via a conducting graphite particle. This system catalyzes the "water-gas shift" reaction with a much higher efficiency than the technologies currently used in industry (60). In contrast, the ability of Hyd-1 to oxidize H_2 in the presence of O_2, along with its great stability on a graphite surface, makes it an appropriate anode catalyst for small enzyme-based fuel cells.

REFERENCES

1. Vignais, P. M., and Billoud, B. (2007) *Chem. Rev.* **107,** 4206–4272
2. Fontecilla-Camps, J. C., Volbeda, A., Cavazza, C., and Nicolet, Y. (2007) *Chem. Rev.* **107,** 4273–4303
3. Lamle, S. E., Albracht, S. P., and Armstrong, F. A. (2004) *J. Am. Chem. Soc.* **126,** 14899–14909
4. Vincent, K. A., Parkin, A., Lenz, O., Albracht, S. P., Fontecilla-Camps, J. C., Cammack, R., Friedrich, B., and Armstrong, F. A. (2005) *J. Am. Chem. Soc.* **127,** 18179–18189
5. van Gastel, M., Stein, M., Brecht, M., Schröder, O., Lendzian, F., Bittl, R., Ogata, H., Higuchi, Y., and Lubitz, W. (2006) *J. Biol. Inorg. Chem.* **11,** 41–51
6. Lubitz, W., Reijerse, E., and van Gastel, M. (2007) *Chem. Rev.* **107,** 4331–4365
7. van Gastel, M., Fichtner, C., Neese, F., and Lubitz, W. (2005) *Biochem. Soc. Trans.* **33,** 7–11
8. Jones, A. K., Lamle, S. E., Pershad, H. R., Vincent, K. A., Albracht, S. P., and Armstrong, F. A. (2003) *J. Am. Chem. Soc.* **125,** 8505–8514
9. Caffrey, S. M., Park, H. S., Voordouw, J. K., He, Z., Zhou, J., and Voordouw, G. (2007) *J. Bacteriol.* **189,** 6159–6167
10. Burgdorf, T., Lenz, O., Buhrke, T., van der Linden, E., Jones, A. K., Albracht, S. P., and Friedrich, B. (2005) *J. Mol. Microbiol. Biotechnol.* **10,** 181–196
11. Olson, J. W., and Maier, R. J. (2002) *Science* **298,** 1788–1790
12. Maier, R. J., Olczak, A., Maier, S., Soni, S., and Gunn, J. (2004) *Infect. Immun.* **72,** 6294–6299
13. Cracknell, J. A., Wait, A. F., Lenz, O., Friedrich, B., and Armstrong, F. A. (2009) *Proc. Natl. Acad. Sci. U.S.A.* **106,** 20681–20686
14. Buhrke, T., Lenz, O., Krauss, N., and Friedrich, B. (2005) *J. Biol. Chem.* **280,** 23791–23796
15. Sawers, G. (1994) *Antonie Leeuwenhoek* **66,** 57–88
16. Sawers, R. G., Ballantine, S. P., and Boxer, D. H. (1985) *J. Bacteriol.* **164,** 1324–1331
17. Sawers, R. G., and Boxer, D. H. (1986) *Eur. J. Biochem.* **156,** 265–275
18. Ballantine, S. P., and Boxer, D. H. (1986) *Eur. J. Biochem.* **156,** 277–284
19. Menon, N. K., Robbins, J., Wendt, J. C., Shanmugam, K. T., and Przybyla, A. E. (1991) *J. Bacteriol.* **173,** 4851–4861
20. Sargent, F., Ballantine, S. P., Rugman, P. A., Palmer, T., and Boxer, D. H. (1998) *Eur. J. Biochem.* **255,** 746–754
21. Dubini, A., Pye, R. L., Jack, R. L., Palmer, T., and Sargent, F. (2002) *Int. J. Hydrogen Energy* **27,** 1413–1420
22. Giel, J. L., Rodionov, D., Liu, M., Blattner, F. R., and Kiley, P. J. (2006) *Mol. Microbiol.* **60,** 1058–1075

23. Richard, D. J., Sawers, G., Sargent, F., McWalter, L., and Boxer, D. H. (1999) *Microbiology* **145,** 2903–2912
24. Atlung, T., Nielsen, A., and Hansen, F. G. (1989) *J. Bacteriol.* **171,** 1683–1691
25. Brøndsted, L., and Atlung, T. (1994) *J. Bacteriol.* **176,** 5423–5428
26. King, P. W., and Przybyla, A. E. (1999) *J. Bacteriol.* **181,** 5250–5256
27. Laurinavichene, T. V., and Tsygankov, A. A. (2001) *FEMS Microbiol. Lett.* **202,** 121–124
28. Adams, M. W., and Hall, D. O. (1979) *Biochem. J.* **183,** 11–22
29. Armstrong, F. A. (2005) *Curr. Opin. Chem. Biol.* **9,** 110–117
30. Vincent, K. A., Parkin, A., and Armstrong, F. A. (2007) *Chem. Rev.* **107,** 4366–4413
31. Casadaban, M. J., and Cohen, S. N. (1979) *Proc. Natl. Acad. Sci. U.S.A.* **76,** 4530–4533
32. Hamilton, C. M., Aldea, M., Washburn, B. K., Babitzke, P., and Kushner, S. R. (1989) *J. Bacteriol.* **171,** 4617–4622
33. Ballantine, S. P., and Boxer, D. H. (1985) *J. Bacteriol.* **163,** 454–459
34. Léger, C., and Bertrand, P. (2008) *Chem. Rev.* **108,** 2379–2438
35. Léger, C., Elliott, S. J., Hoke, K. R., Jeuken, L. J., Jones, A. K., and Armstrong, F. A. (2003) *Biochemistry* **42,** 8653–8662
36. Bard, A., and Faulkner, L. R. (2000) *Electrochemical Methods: Fundamentals and Applications,* Second Ed., Wiley, Chichester, UK
37. Stoll, S., and Schweiger, A. (2006) *J. Magn. Reson.* **178,** 42–55
38. Léger, C., Jones, A. K., Albracht, S. P. J., and Armstrong, F. A. (2002) *J. Phys. Chem. B* **106,** 13058–13063
39. Reda, T., and Hirst, J. (2006) *J. Phys. Chem. B* **110,** 1394–1404
40. Armstrong, F. A., and Albracht, S. P. (2005) *Philos. Transact. A Math. Phys. Eng. Sci.* **363**
41. Albracht, S. P. J., Kalkman, M. L., and Slater, E. C. (1983) *Biochim. Biophys. Acta* **724,** 309–316
42. Cammack, R., Kovacs, K. L., McCracken, J., and Peisach, J. (1989) *Eur. J. Biochem.* **182,** 363–366
43. Saggu, M., Zebger, I., Ludwig, M., Lenz, O., Friedrich, B., Hildebrandt, P., and Lendzian, F. (2009) *J. Biol. Chem.* **284,** 16264–16276
44. Cammack, R., Patil, D., Aguirre, R., and Hatchikian, E. C. (1982) *FEBS Lett.* **142,** 289–292
45. Brugna-Guiral, M., Tron, P., Nitschke, W., Stetter, K. O., Burlat, B., Guiglierelli, B., Bruschi, M., and Giudici-Orticoni, M. T. (2003) *Extremophiles* **7,** 145–157
46. Lalla-Maharajh, W. V., Hall, D. O., Cammack, R., Rao, K. K., and Le Gall, J. (1983) *Biochem. J.* **209,** 445–454
47. DerVartanian, M. E., Menon, N. K., Przybyla, A. E., Peck, H. D., Jr., and DerVartanian, D. V. (1996) *Biochem. Biophys. Res. Commun.* **227,** 211–215
48. Teixeira, M., Moura, I., Xavier, A. V., Huynh, B. H., DerVartanian, D. V., Peck, H. D., Jr., LeGall, J., and Moura, J. J. (1985) *J. Biol. Chem.* **260,** 8942–8950
49. Romão, C. V., Pereira, I. A., Xavier, A. V., LeGall, J., and Teixeira, M. (1997) *Biochem. Biophys. Res. Commun.* **240,** 75–79
50. Hatchikian, C. E., Traore, A. S., Fernandez, V. M., and Cammack, R. (1990) *Eur. J. Biochem.* **187,** 635–643
51. Albracht, S. P. J., Albrecht-Ellmer, K. J., Schmedding, D. J. M., and Slater, E. C. (1982) *Biochim. Biophys. Acta* **681,** 330–334
52. Albracht, S. P. J., Van der Zwaan, J. W., and Fontijn, R. D. (1984) *Biochim. Biophys. Acta* **766,** 245–258
53. Albracht, S. P. J., Fontijn, R. D., and Van der Zwaan, J. W. (1985) *Biochim. Biophys. Acta* **832,** 89–97
54. Larminie, J., and Dicks, A. (2003) *Fuel Cell Systems Explained*, 2nd Ed., Wiley, Chichester, UK
55. Goldet, G., Wait, A. F., Cracknell, J. A., Vincent, K. A., Ludwig, M., Lenz, O., Friedrich, B., and Armstrong, F. A. (2008) *J. Am. Chem. Soc.* **130,** 11106–11113
56. Parkin, A., Goldet, G., Cavazza, C., Fontecilla-Camps, J. C., and Armstrong, F. A. (2008) *J. Am. Chem. Soc.* **130,** 13410–13416
57. Atlung, T., Knudsen, K., Heerfordt, L., and Brøndsted, L. (1997) *J. Bacteriol.* **179,** 2141–2146
58. Bernhard, M., Benelli, B., Hochkoeppler, A., Zannoni, D., and Friedrich, B. (1997) *Eur. J. Biochem.* **248,** 179–186
59. Menon, N. K., Chatelus, C. Y., Dervartanian, M., Wendt, J. C., Shanmugam, K. T., Peck, H. D., Jr., and Przybyla, A. E. (1994) *J. Bacteriol.* **176,** 4416–4423
60. Lazarus, O., Woolerton, T. W., Parkin, A., Lukey, M. J., Reisner, E., Seravalli, J., Pierce, E., Ragsdale, S. W., Sargent, F., and Armstrong, F. A. (2009) *J. Am. Chem. Soc.* **131,** 14154–14155

How *Escherichia coli* Is Equipped to Oxidize Hydrogen under Different Redox Conditions

Michael J. Lukey, Alison Parkin, Maxie M. Roessler, Bonnie J. Murphy, Jeffrey Harmer, Tracy Palmer, Frank Sargent and Fraser A. Armstrong

J. Biol. Chem. 2010, 285:3928-3938.
doi: 10.1074/jbc.M109.067751 originally published online November 16, 2009

This paper is available online at www.jbc.org

THE JOURNAL OF BIOLOGICAL CHEMISTRY VOL. 285, NO. 26, p. 20421, June 25, 2010

VOLUME 285 (2010) PAGES 10993–11002
DOI 10.1074/jbc.A109.070797

Kinetic evaluation of cell membrane hydrolysis during apoptosis by human isoforms of secretory phospholipase A_2.

Erin D. Olson, Jennifer Nelson, Katalyn Griffith, Thaothanh Nguyen, Michael Streeter, Heather A. Wilson-Ashworth, Michael H. Gelb, Allan M. Judd, and John D. Bell

PAGE 10993:

The grant information footnote for Dr. Michael Gelb should read as follows: This work was supported by National Institutes of Health Grant R37 HL36235.

VOLUME 285 (2010) PAGES 13012–13021
DOI 10.1074/jbc.A109.037747

DAXX is a new AIRE-interacting protein.

Alessandra Meloni, Edoardo Fiorillo, Denise Corda, Federica Incani, Maria Luisa Serra, Antonella Contini, Antonio Cao, and Maria Cristina Rosatelli

Dr. Meloni's first name was misspelled. The correct spelling is shown above.

VOLUME 282 (2007) PAGES 22544–22550
DOI 10.1074/jbc.A110.702304

Biochemical characterization of the ATPase and helicase activity of UAP56, an essential pre-mRNA splicing and mRNA export factor.

Jingping Shen, Lingdi Zhang, and Rui Zhao

PAGE 22546:

Under the heading "Helicase Reaction," line 4: "2 mM $MgCl_2$" should be inserted after "65 mM NaCl."

VOLUME 285 (2010) PAGES 17253–17262
DOI 10.1074/jbc.A110.102228

Prolyl 3-hydroxylase 1 null mice display abnormalities in fibrillar collagen-rich tissues such as tendons, skin, and bones.

Janice A. Vranka, Elena Pokidysheva, Lauren Hayashi, Keith Zientek, Kazunori Mizuno, Yoshihiro Ishikawa, Kerry Maddox, Sara Tufa, Douglas R. Keene, Robert Klein, and Hans Peter Bachinger

PAGE 17257:

Fig. 2, line 9 should read: *F*, a projection through a 350 nm thick section of longitudinally sectioned P3H1 null tendon from which the tilt series (supplemental Fig. S1) was collected.

VOLUME 285 (2010) PAGES 3928–3938
DOI 10.1074/jbc.A109.067751

How *Escherichia coli* is equipped to oxidize hydrogen under different redox conditions.

Michael J. Lukey, Alison Parkin, Maxie M. Roessler, Bonnie J. Murphy, Jeffrey Harmer, Tracy Palmer, Frank Sargent, and Fraser A. Armstrong

PAGE 3931, FIG. 1:

The wrong image was inadvertently printed. The correct Fig. 1 is shown below.

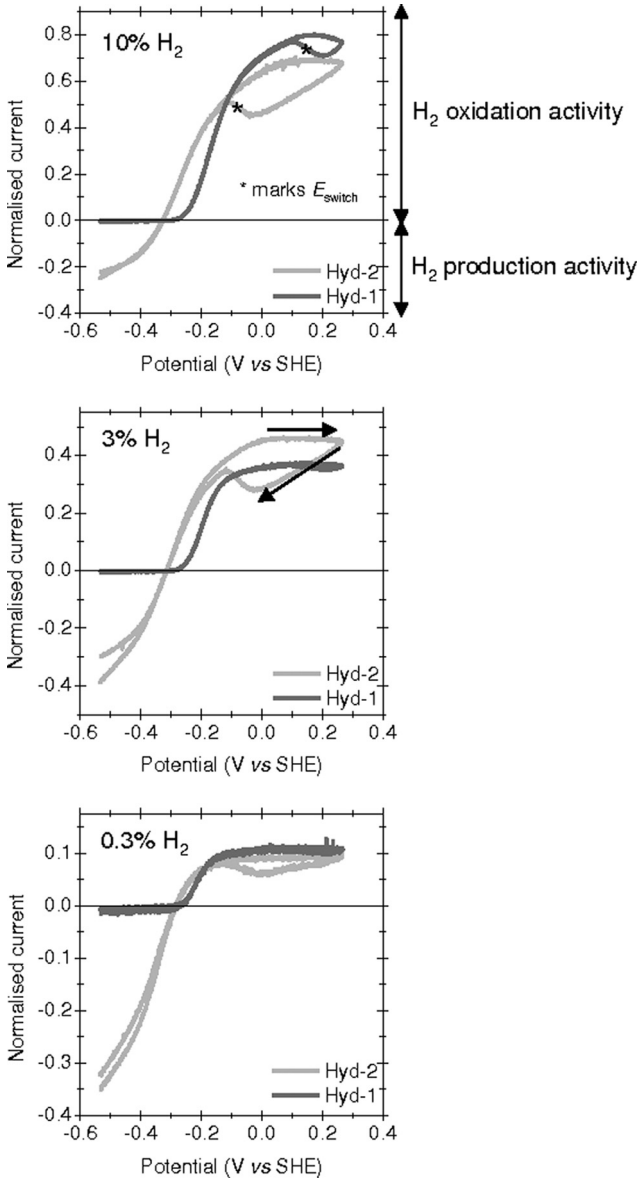

We suggest that subscribers photocopy these corrections and insert the photocopies in the original publication at the location of the original article. Authors are urged to introduce these corrections into any reprints they distribute. Secondary (abstract) services are urged to carry notice of these corrections as prominently as they carried the original abstracts.